Catalysis Science & Technology

Accepted Manuscript

ROYAL SOCIETY OF CHEMISTRY

www.rsc.org/catalysis

Synergistic effect of $PtSe_2$ and graphene sheet supported by TiO_2 as cocatalysts synthesized via microwave techniques for improved photocatalytic activity

Kefayat Ullah[1], Shu Ye[1], Zhu Lei[1], Kwang-Yeon Cho[2], Won-Chun Oh[1] *

[1]*Department of Advanced Materials Science & Engineering, Hanseo University, Seosan-si, Chungnam-do, Korea, 356-706*

[2] *Korea Institutes of Ceramic Engineering and Technology, Seoul 153-801, Korea*

Abstract:

Here we report a new composite material consisting of TiO_2 nanoparticles grown in the presence of a layered $PtSe_2$/graphene hybrid as a high-performance photocatalyst material. The heterogeneous $PtSe_2$-graphene/TiO_2 nanocomposites were successfully synthesized through a facile and fast microwave assisted method. The prepared composites were characterized through X-ray diffraction (XRD), scanning electron microscopy (SEM) with an energy dispersive X-ray (EDX) ,transmission electron microscopy (TEM), Raman spectroscopic analysis, X-ray photoelectron spectroscopy (XPS), UV-vis absorbance spectra and UV-vis diffuse reflectance spectra (DRS) analysis were obtained. The catalytic behavior was investigated through the decomposition of rhodamine B (Rh.B) as a standard dye and Texbrite MST-L as an industrial dye. This extraordinary photocatalytic activity arises from the positive synergetic effect between the $PtSe_2$ and graphene components in this heterogeneous photocatalyst. In this study the graphene behaves as electron transfer, collector, contributor and a source of active adsorption sites respectively. The optical properties were also observed to be effected by the different weight % of graphene in the composites by observing their respective band gaps from DRS spectra.

Key words: XPS; Microwave; Texbrite MST-L; nanocomposite; photocatalysis

* Corresponding author
E-mail: wc_oh@hanseo.ac.kr
Tel: +82-41-660-1337, Fax:+82-41-688-3352

Introduction:

Since the discovery of graphene and its uses in the field of photocatalysis, scientists has been devoted a lot of research to understand and explore the role of this peculiar material. While graphene is a nanomaterial with high electron mobility and elevated conductivity [1-2]. It has been reported that bare graphene, graphene oxide or the combination with other semiconductor materials can be used as useful catalyst materials. The result obtained from these researches greatly highlights the importance of degree of oxidation of graphite sheet which greatly influences the catalytic performance [3-4]. The combination of graphene oxide with other photocatalyst materials such as, $BiVO_4$, $PtSe_2$, CdS/ZnO, TiO_2 etc, have been considered to study the photocatalytic effect and enhanced catalytic activities were claimed [5-9]. The main theme of these ideas is to develop graphene based semiconductor materials which collect maximum part of the solar spectrum as energy source. In this context many scientist consider metal or metal complexes supported by organic dyes as a light harvesters to absorb light from the solar spectrum and inject electron to the conduction band of semiconductor materials. A similar approach has been applied to graphene oxide as light harvester to study the visible light photocatalytic activity combined with metal or semiconductor materials [10-14]. In particular, owing to unique sp^2 hybrid carbonated network, graphene based materials has attracted considerable attention because of the high thermal conductivity (~ 5000 W m^{-1} K^{-1}), excellent charge mobility at room temperature (200 000 cm2 V^{-1} s^{-1}), and extremely high theoretical specific surface area (~2600 m^2/g) [15-16]. These excellent properties make graphene as an excellent material in photocatalyst to increase the charge transfer separation of generated electron and holes. The potential application of graphene-based photocatalysts to improve the efficiency of solar energy conversion has been explored [17-20].

The motive for the improved photocatalytic mechanism can be divided into four categories, electron hole pair recombination time, support material to act as catalyst and provide adsorption cites, modification of the energy gap/proper photo responsive effect and the use of cocatalyst to act as reaction centre for suitable catalytic effect [21]. Recently much attention has been devoted to the photocatalytic effect of graphene based materials by altering the band gap of the composites to extend the light response in visible range [22-24]. For example Lee *et al* have verified the modification of the energy gap in graphene based anatase TiO_2 nanocomposite. The

improved catalytic property has been attributed to the red shift of the band edge by providing a precise band gap in the visible range and allows enhanced absorption of light [25]. Similarly Zhang *et al* studied the visible light response of large band gap semiconductor ZnS/graphene oxide and observed enhanced catalytic effect [26]. Conversely, combination of graphene alters the optical properties and increases the visible light response of the composites. Another approach, Z-scheme catalyst system has been introduced to consider graphene as an electron mediator between two semiconductor photocatalyst [27]. The transfer of electron in the Z scheme system between two catalysts is the main feature for producing H_2 oxygen or other mineral products. The main challenge in manufacturing a solid state electron mediator is to achieve a state of dynamic equilibrium between the electron acceptor and donator, to remain unchanged during reaction and provide a greater interfacial contact. Similarly ternary CdS–graphene–TiO_2 hybrids (CdS–GR–TiO_2) have been prepared through an in situ approach on the surface of graphene oxide (GO). It is found that the introduction of the third-component TiO_2 can sustain the porosity of the samples, tuning of the band gap, increase the surface area, and facilitate the charge transfer, thus extending the lifetime of photogenerated carriers [28].

In spite of these promising results, the main problems which also alter the photocatalytic properties are agglomeration of nanoparticles on graphene sheet, which causes a poor interfacial contact between nanoparticles and graphene surface. Thus homogenous distribution of nanoparticles and utmost interfacial contact with graphene is essential factor to enhance the catalytic activity. This will help to improve charge transfer effect between catalyst nanoparticles and graphene sheet under light illumination. It has been found that the coupling of small energy band graphene based semiconductor with large energy band photocatalyst material extend the light response to visible region due to possible synergistic effect between the composites materials [29-30].

In this work we report a fast and facile route for the preparation of layered $PtSe_2$-graphene supported TiO_2 photocatalyst through microwave assisted techniques. In this process, graphene oxide is mixed with Pt and Se precursor material, and the resulting solution is irradiated through microwave for 300 sec. followed by mixing of TiO_2 precursor material under appropriate condition. During microwave irradiation, partial reduction of graphene oxide into graphene and attachment of $PtSe_2$ and TiO_2 nanoparticles on graphene sheet are observed in ethylene glycol.

The photo catalytic activities of as prepared nanocomposites were tested with Rh. B as a standard and Texbrite MST-L as an industrial organic pollutant under UV/Vis light.

2. Experimental Sections:

2.1. Materials

Titanium (IV) n-butoxide (TNB, $C_{16}H_{36}O_4Ti$) used as a titanium precursor was purchased from Samchun Pure Chemical Co. Ltd., Korea. Hydrogen hexachloroplatinate (IV) hydrate ($H_2PtCl_6.\ nH_2O$ n=5.5) and Selenium powder (Se) were purchased from Kojima Chemical Co. Ltd., Japan. Rhodamine B (Rh. B, $C_{28}H_{31}ClN_2O_3$) was used as a model pollutant, purchased from Samchun Pure Chemical Co. Ltd., Korea. Ethylene glycol was purchased from Dae-Jung Chemical and Metals Co. Ltd Korea. Texbrite MST-L was purchased from Texchem Korea Co. Ltd. All the chemicals were used without further purification.

2.2. Synthesis of Graphene Oxide

Graphene oxide was prepared through modified Hummers Offman method reported in our previous work [31-32]. In short, 20 g of natural graphite powder were mixed with conc. H_2SO_4 (230ml) at 0˚C with constant magnetic stirring. In the 2nd step, 30 g of $KMnO_4$ was slowly added to the flask and the temperature was kept below 15˚C. The resulting mixture was stirred at 35 ˚C until it became pale brownish, and it was then diluted to 150 ml using de-ionized (DI) water and kept stirring at below 90 ˚C. After adding water, the container was sealed and kept at 100 ˚C with vigorous stirring for 30 minutes, followed by the addition of 20 % H_2O_2, drop by drop, within 5 minutes. The mixture was then washed several times with water, acetone and 10 % HCl solution to eliminate residual metal ions. The mixture was then heat treated in a dry oven at 90˚C for 12 h to obtain graphite oxide powder. For the preparation of graphene oxide, 200 mg of graphite oxide powder were mixed in 200 ml DI water (1mg/ml), stirring for 30 minutes and ultrasonicated for 1 h. The resulting solutions were filtered and washed several times with hot water and kept in a dry oven for 8 h to achieve graphene oxide powder.

2.3. Synthesis of Platinium Selenide

Platinium selenide was synthesized through fast microwave assiatted techniques. In a typical synthesis 1.5 g of anhydrous sodium sulfite (Na_2SO_3) and 0.3 g of crude selenium (Se) powder was mixed together in 200 ml of ethylene glycol under vigourous magnetic stirring. The solution was stirred vigourously for 1 hr at 60 ^oC to ensure homogenous mixture and attain selenium salt.

In the next step 0.5 mmol of hydrogen hexachloroplatinate ($H_2PtCl_6.nH_2O$ n=5.5) was added to the abve solution and stirred for 30 minutes to attain a stable solution. The obtained solution was finally transferred to 500 ml reaction vessel placed in conventional microwave oven. Th solution was then irradaitted with microwave for 300 s, with peroidic on off setting after 5s. The mixture was then cooled at room temperature, filtered with watman filte rpaper and hea treated for 6 h at 90 ^oC to obain a dark brown $PtSe_2$ powder.

2.4. Synthesis of $PtSe_2$-graphene supported TiO_2 photocatalyst

$PtSe_2$/graphene nanocomposites were obtained by following the above method. A borosilicate glass sealed reaction vessel specially designed for microwave techniques having a diameter of 8 cm and height 10 cm was used. Graphene oxide 200 mg and desired amount of TNB as titanium precursor was dispersed in 300 ml ethylene glycol for 30 minutes to attain a homogenous mixture to form a solution A. In the next step 1 g of anhydrous sodium sulfite (Na_2SO_3) and 0.2 g of crude selenium powder (Se) were vigourously stirred in 100 mL of ethylene glycol for 30 min to attain a homogenous solution. Followed by the addition of desired amount of hydrogen hexachloroplatinate ($H_2PtCl_6nH_2O$ n=5.5) with vigorous stirring for 1 h at 35 ^oC to ensure the homogenous mixing to form a stable suspension B. A and B were mixed together stirred for several minutes and transferred into a 500 mL reaction vessel placed in a conventional microwave oven. The solution is then irradiated with microwave for 5 sec. on and off for 300 sec., and cooled at room temperature filtered with whatman filter paper. The resultant powder was washed 3 times with distilled water and transferred into a dry oven for 6 h at 90 °C. The powder was then heat treated at 500 °C for 1 h in electric furnace. The weight ratios of GO to $PtSe_2$ and TiO_2 were taken as 1%, 2.5%, 3.5% and 4.5 %, the obtained samples were labeled as $PtSe_2$-GT1, $PtSe_2$-GT2, $PtSe_2$-GT3, $PtSe_2$-GT4, respectively.

2.5. Photocatalytic Studies

The photocatalytic activity of the as-prepared $PtSe_2$-graphene supportted TiO_2 nanocomposites were evaluated by the degradation of Rh. B and Texbrite MST-L as an organic dyes under UV/Vis light. Xenon lamp 12 W served as the simulated visible light source. In each run10 mg of $PtSe_2$-graphene/TiO_2 catalytic samples were taken in 80 ml solution of Rh. B (0.1mg $ml^{-1)}$. To obtain adsorption desorption equilibrium the solution was kept under dark for 2 h. Before the Xenon lamp was switched on a sample was collected from the solution and kept in

a centrifuge at 10,000 rpm for the removal of solid material. Afterwards, the Xenon lamp was switched on and samples were collected periodically. At given time intervals, the collected samples were centrifuged for 10 minutes instantly to remove the solid material for further analysis. Each photocatalyst in the composite was irradiated for 150 minutes to compare their catalytic efficiencies.

A similar procedure is used to measure the photocatalytic activity of the $PtSe_2$-graphene/TiO_2 nanocomposite, using UV light for the degradation of Texbrite MST-L. The photocatalytic behavior of the samples was analyzed through the absorbance spectrometry with a UV/Vis spectrophotometer (Optizen POP, Mecasys, Korea).

2.6. Instrumentation

The fabrication of the samples were carried out in the Microwave oven (RE-406B) 700 W Samsung Korea Ltd. LED lamp (8W, Fawoo, Lumidas-H, Korea) was used at a distance of 90 mm from the solution in the dark box for the ivestigation of catalytic properties. UV light source model No: VL-4. LC 365nm, 8 W, Villber Lourmat, France) was used. To determine the crystal phase and the composition of the as-prepared $PtSe_2$-graphene supported TiO_2 samples, XRD characterization was carried out at room temperature using XRD (Shimata XD-D1, Japan) with Cu Kα radiation (λ=1.54056 Å) in the range of 2θ = 10-80 ^{o} at a scan speed of 1.2 ^{o} m^{-1}. A SEM (JSM-5200 JOEL, Japan) was used to observe the surface state and morphology of the prepared nanoparticles. The morphology of the samples was studied with an Energy dispersive X-ray spectroscopy (EDX), which was also employed for elemental analysis. Transmission electron microscopy (TEM, JEOL, JEM-2010, Japan) was used to observe the surface state and structure of the photocatalyst composites at an acceleration voltage of 200 kV. TEM was also used to examine the size and distribution of the $PtSe_2$ and TiO_2 nanoparticles on the graphene sheet. X-ray photoelectron spectroscopy (XPS) was performed using VG scientific VISACA lab 2000, and a monochromatic Mg X-ray radiation source. Survey (wide scan) spectra and high-resolution spectra of C1s, and the element contained within sample, were recorded. C/O ratios were evaluated from the wide scan spectra, by using relative sensitivity factors. Diffuse reflectance spectra were obtained by using a scan UV/Vis spectrophotometer (Neosys-2000) equipped with an integrating sphere assembly. Raman spectra of the samples were observed using a spectrometer (Jasco Model Name NRS-3100) with an excitation laser wavelength of 532.06 nm.

The decomposition kinetics for the photocatalytic activity was measured by using a spectrometer (Optizen POP, Mecasys, Korea).

3. Results and Discussions

3.1. Growth and characterization

The microwave assisted fabrication of the nanocomposites is depicted in scheme 1. Microwave synthesis is solvent limited techniques and usually need polar solvent. Therefore ethylene glycol was selected as a solvent to absorb microwave energy and localized overheat which causes decomposition. Microwave techniques are advantageous over other synthesis techniques because of less amount of solvent and clear reaction profile causes small waste. A short reaction time is needed which help to save electricity and extra cooled reflux water. Another advantage of closed reaction vessel for short time prevents releasing toxic gases to environment [33-34]. Microwaves act as high frequency electric fields and will generally heat any material having movable electric charges, such as in solid state conducting ions, polar molecules in a solvent. Polar solvents are heated as their component molecules are forced to rotate with the field and lose energy in collisions. Conductors and semiconductor materials produce heat when ions or electrons within them form an electric current and energy is lost due to the electrical resistance of the material. This high frequency waves generates a localized hot spot with extremely high temperature and pressure and accelerate the nanoparticles and simultaneous attachment occur [35-36]. Structural features and for the identification of crystalline phases of the $PtSe_2$-graphene/TiO_2 nanocomposites with varying amount of graphene were analyzed by XRD as shown in figure 1. The bare $PtSe_2$ and $PtSe_2$ in the composites had similar diffraction pattern that corresponds to hexagonal crystal phase (JCPDS PDF#: 00-065-3374) exhibit the characteristic diffraction peaks at (001), (011), (012), (110), (111), (201), (202), (113), (121) and (122) reflections. The intensity of the $PtSe_2$ peaks is very high as compared to $PtSe_2$-graphene/TiO_2 nanocomposites. The suppression of the peaks confirms the minute development of the crystalline phases on graphene sheet. The intensity variation of the diffraction peaks for the nanocomposites also verify the increase amount of graphene and suppression of the crystalline phases. The interaction of the nanoparticles with graphene sheet creates phonon confinement effect which decreases the probability of formation of spherical particles. Decrease in intensity peaks suggest that the lattice structure of $PtSe_2$ is distorted by the

interaction with GO [37-38]. The $PtSe_2$ are found to be sheet like from the TEM results which also evident this suppression of the peak. The TiO_2 diffraction peak (101) and graphene (002) peak are located at same 2Θ values. Therefore it is difficult to distinguish both peaks as a result of intense diffraction from TiO_2 (002) plane. The nanocomposite contains characteristics reflection (101), (004), (200), (105), (211), and (220) that corresponds to the anatase crystal phase (JCPDS PDF#: 00-021-1272).

EDX spectra were carried out to obtain the micro elemental analysis of microwave assisted $PtSe_2$-graphene/TiO_2 nanocomposites as shown in figure 2. In the whole spectra, C elemental peak derived from the graphene sheet. The strong Kα and K_β peaks from Se element appear at 11.2 and 12.4 KeV while moderate Kα peak from O element appear at 0.54 KeV [30]. The titanium and oxygen in the figure arise from the TiO_2 precursor material. The strong Kα and K_β peaks from the Ti element appear at 4.5 and 4.9 KeV. Figure 2 also confirms the presence of Pt in the composite with the strong peaks at 2.3 KeV [39]. Table 1 lists the numerical results of the EDX quantitative microanalysis of the samples. There were some small impurities, which were attributed to the starting experiment for the oxidation of graphite to obtain graphene oxide.

The surface morphologies of the sample $PtSe_2$-GT3 nanocomposite were examined using SEM as function of graphene oxide content as depicted in figure 3. The sample was analyzed at different regions with same magnification to examine the overall morphology of the composite. Figure 3 (a) ascribed the SEM image of the $PtSe_2$-GT3 sheet with lower magnification. From this figure the overall structure can be clearly predicted that graphene is plate like structure broken off in different direction. The morphology of the graphene is observed as a crumbling texture which reflects its layer structure. After microwave treatment, the sheet morphology is retained and the surfaces are covered with $PtSe_2$ sheet and TiO_2 nanoparticles as shown in figure 3(b-c). The same plate like morphology can be seen in figure 3(d-e). Because of the presence of oxygen functionalities on the surface of graphene sheet, electrostatic force arises among them in the form of Van dar Walls interaction that tends graphene sheet to aggregate back to graphitic structure. Attachment of nanoparticles on graphene sheet is helpful to overcome these interactions [40]. The graphene sheet acts like a support material which may be advantageous to supply a path for the generated electron and as a result will improve the photocatalytic behavior of the nanocomposites.

The microstructure of the nanocomposites was studied using TEM for further confirmation of the morphology and shape of the $PtSe_2$-GT3 sample. The TEM image has been depicted in figure 4 (a-e) with different magnification. In figure 4 (a-b), it can be seen that the nanoparticles of TiO_2 are partially agglomerated on the surface $PtSe_2$ and graphene sheet. The $PtSe_2$ seems to form a bridge like support between TiO_2 and graphene sheet. These results are in good agreement with the theoretical reports [41-42]. It is clear from figure 4 (c-d) that the two dimensional structure of the graphene sheet is retained with partial agglomeration and the TiO_2 nanoparticles are seen to be spherical in shape resides on $PtSe_2$ nanosheet and graphene. Figure 4 (e) with 20 nm resolution shows TEM image of the resulting $PtSe_2$-GT3 composite in which the layer $PtSe_2$ act as novel support that is mostly decorated with TiO_2 nanoparticles. Thus it can be inferred that the close neighboring of TiO_2, $PtSe_2$ and graphene components achieved through microwave assisted techniques is supposed to favor the victorial transfer of photoexcited electrons from $PtSe_2$ to TiO_2 or graphene sheets, thus increasing the charge separation effect and catalytic efficiency [43].

XPS was carried out for the qualitative analysis of the $PtSe_2$-GT3 nanocomposite containing $PtSe_2$, TiO_2 and graphene. The XPS survey spectrum had peaks corresponds to Pt, Se, O, C and Ti consistent with the formation of $PtSe_2$-graphene/TiO_2 nanocomposites as shown in figure 5 (f). Figure 5 (a) shows the C1s spectra of the carbon presented in the composites. The C1s has a strong peak located at around 284.1 eV and a slight peak at 289.1 eV. These binding energies corresponds to C-O, and C=O functional groups. These results reveal that our nanocomposites still contains some partial oxygen functional groups. The peak position in figure 5 (b) of Ti 2p corresponds to that of the Ti^{4+} oxidation state. During thermal heating process, Ti 2p peak becomes narrow and the peak position of Ti $2p_{3/2}$ moves, indicating that there is also little Ti exists in low valence (Ti^{3+}) form [44]. The presence of oxygen functional groups may increase the light absorption towards the visible region [45]. As it is clear that the O1s photoelectron kinetic energies are smaller than those of the C1s, thus the sampling depth is smaller, and therefore the O1s spectra are slightly more surface specific. We have assigned in figure 5(c) the O1s peak at 532.1 eV to contributions from C=O and O-C–OH groups this means after heat treatment the conversion to other chemical species may be possible [46-47]. The remaining peak at 534.7eV indicates that C–OH group is still appearing. Assuming that the reduction of

remaining C–OH groups in reduced graphene oxide is very difficult or it may not possible at our heat treated condition [48]. Selenium 3d core level peak were confirmed at 54.1 eV form the high resolution scan spectra as shown in figure 5 (d). The author assume that their XPS Pt4f spectra invariably involve 2 different platinum chemical species as shown in figure 5(e) wich produces a single peak each, any given platinum chemical species in fact produces 2 spin–orbit split (Pt4f7/2 and Pt4f5/2) Pt4f peaks corresponds to (74.1 and 77.3) eV [49-50]. In figure 5 (e) both the spin–orbit multiplicity and chemical state multiplicities of the Pt4f peaks, indeed; one invariably expects a branching ratio and energy separation for both the peaks Pt4f7/2 and Pt4f5/2 of 3.2 eV [51].

Raman spectroscopy was used to analyze the structural properties of the $PtSe_2$-graphene/TiO_2 nanocomposites. Figure 6 (A-B) depicted the micro Raman spectra of GO and our nanocomposites with G band and D band correspond to the vibration of carbon atom in disorder or defects site and in plane vibration of sp^2 bonded carbon atoms respectively [52]. The intensities of peaks depend on defects concentration. The difference in the Raman band intensity or shift provides information about the nature of the defects and C-C bonds [53]. The characteristics D and G bands appear at 1354 cm^{-1} and 1590 cm^{-1} respectively. The peaks observed below 600 cm^{-1} may be assigned to metallic component in the composites crystal. The peaks around 200 cm^{-1} to 300 cm^{-1} wave number are attribute to some Se^o trigonal phase. And the peaks around 410 cm^{-1} and 510 cm^{-1} seems to be associated with the anatase TiO_2 [54-55]. The defects can be reflected by the intensity ratio of the corresponding D to G band. The calculate ratio of the intensities from D to G band were found to be ~0.960. This value is much smaller than that of graphene oxide in figure 6 (A). The decrease in the I_D/I_G ratio is clear evidence of the increase number of graphene layers. Moreover, the lower I_D/I_G ratio expresses an improved defect repair mechanism [56].

The search for the design of new photocatalyst materials which utilizes the maximum part of solar energy spectrum is very important. For the decontamination or elimination of environmental pollutant needs an ideal photocatalyst have maximum efficiency in both UV and visible rang of the electromagnetic spectrum. In this context we carried out the absorption spectroscopy of our nanocomposites and try to understand the response of our nanocomposites to electromagnetic spectrum. The DRS spectra depicted in figure 7 clearly reveals that our

nanocomposites mainly absorb in the visible light of electromagnetic spectrum. The overall spectra looks like the ordinary carbon based semiconductor materials [57]. From the spectra it is clearly observed that bare TiO_2 has absorbance in the UV region because of the intrinsic band gap energy absorption (3.2 eV). After the attachment of $PtSe_2$ and graphene the absorption edge shifts towards the visible region. Due to carbonated structure of graphene, the unpaired π electron may cause the interaction with metal nanoparticles. Such interaction may cause the shift in the band edges and may increase the light absorption towards the visible region [58]. Lee et al also observed such kind of effect with titanium nanoparticles and observed the optical response towards the visible region of electromagnetic spectrum [25]. It can be clearly seen that the modification of graphene with platinium selenide results in red shifts in the absorption edges, and moreover, the absorption intensities are significantly increased in the whole visible region, confirming effectively improved light-harvesting activity.

The evaluation of the band gap was carried out using Kubelka Mulk transformation by converting the reflectance plot according to Tauc condition. The following equation was proposed by Tauc, Davis, and Mott [59].

$$(h\nu\alpha)^{1/n} = A(h\nu - E_g) \quad (1)$$

Where h is plank constant, ν is frequency of vibration, α is the absorption coefficient. E_g is band gap and A is proportional constant. The value of the n in the exponent of equation 1 represents the nature of sample transition. i.e., for direct allowed transition n=1/2. In the next step the acquired diffuse reflectance spectrum is converted to Kubelka Mulk transformation. In this calculation the vertical axis is converted to quantity called F(R∞), which is proportional to the absorption coefficient. Thus, the α in the Tauc plot in equation is substituted with the function F(R∞). The actual relational expression becomes

$$(h\nu\, F(R\infty))^2 = A(h\nu - E_g) \quad (2)$$

Using the KM function, the $(h\nu\, F(R\infty))^2$ was plotted against the hν. The curve having $(h\nu\, F(R\infty))^2$ on the horizontal and hν on the vertical axis defines the precise band gap our nanocomposites. The unit of the hν is eV and its relation to the wavelength is well known equation $h\nu = 1240/\lambda$. A line drawn tangent to a point of inflection on the curve and the hν value at that point defines the estimated band gap of the nanocomposites [9, 6, 20]. The obtained plots are given in figure 8. The band gap energies were found to be in order of $PtSe_2$-GT1> $PtSe_2$-

GT2> $PtSe_2$-GT4> $PtSe_2$-GT3 of the $PtSe_2$-graphene/TiO_2 nanocomposites. The corresponding values for approximated band gap are given in table 1 in detail. The difference in the band gap of our nanocomposites is attributed to the distribution of $PtSe_2$ and TiO_2 nanoparticles on the graphene sheet. Similarly the partial agglomeration can also affect the absorption property and hence may result in band gap variation. Another reason for the variation of the band gap may be the different amounts of graphene in the composites, which considerably affects the optical property of $PtSe_2$-graphene/TiO_2 nanocomposites. Therefore, reduction in the band gap is observed for the composites also reported elsewhere [60-61].

3.2. Adsorption properties and proposed photocatalytic mechanism study

The photocatalytic activity of the as-prepared nanocomposite was evaluated by catalytic degradation of Rh. B and Texbrite MST-L as an organic dye UV and visible light irradiation. For the degradation and photocatalysis mechanism important steps are the absorption by the photocatalyst, adsorption of pollutant on the surface of catalyst materials and the fast charge transfer rout to create the radical species to decompose the organic pollutants. In our nanocomposites graphene act as adsorption support materials due to its conjugated structure and two dimensionality. The dye molecule absorbed on the surface of graphene via π-π interaction. [62]. In order to check the adsorption ability of the $PtSe_2$-graphene/TiO_2 nanocomposites, the concentration changes of rhodamine B solution were recorded and were shown in figure 9 (a-c).

In order to attain adsorption-desorption equilibrium, the solution was kept under dark for 2h, after adsorption desorption equilibrium were achieved the solution was kept under visible light chamber. The solution was irradiated with visible light radiation for 30 min. For analysis the sample was withdrawn periodically with 30 min. time interval, the solid material were removed by centrifugation. Dye concentration of the sample was analyzed using UV-visible spectrometer. As shown in figure 9 almost 80 % of the organic dye was degraded by the $PtSe_2$-GT3 sample in 150 minutes. The degradation rate can be seen from the decrease in the intensity peak 554 nm of the Rh. B dye with increasing time interval. The decrease in the concentration and improved catalytic effect can be attributed to the homogenous distribution of TiO_2 and $PtSe_2$ component by providing large number of reaction centres. The metallic nanoparticles on the graphene sheet create a Schottky barrier at the interface with TiO_2 and graphene sheet. Therefore the trapped electrons will transfer and separate the excited molecules absorbed at the interface of

$PtSe_2$ and graphene sheet by retaining the recombination process. This may be helpful to increase the degradation efficiencies of our nanocomposites. In order to test the adsorption ability of the nanocomposites, the concentration changes of Rh. B solution were recorded and shown in figure 9 (d). It can be clearly seen that 80 % of Rh. B was degraded by $PtSe_2$-GT3 nanocomposite. Adsorption of Rh. B was slightly reduced by the incorporation of different wt% of graphene to TiO_2 in the composites. Similar to the above results, loading of TiO_2 slightly reduced the adsorption, while increasing the amount of graphene significantly enhanced the adsorption, which is evident by the $PtSe_2$-GT3 nanocomposite, and describes the optimum loading condition in our nanocomposites.

The kinetic studies were performed on the basis of the degradation rate of the organic dye. The reactions between the dye molecules and the catalyst materials can be expressed by the Langmuir- Hinshelwood model as shown in figure 10 and expressed by the following equation [63].

$$-dC/dt = K_{app}C \qquad (1)$$

Integrating this equation (with the restriction $C = C_0$ at $t = 0$, with C_0 being the initial concentration in the bulk solution after dark adsorption, and t is the reaction time) will lead to the following relation

$$-\ln C_t/C_0 = K_{app}t \qquad (2)$$

where C_t and C_0 are the reactant concentrations at times t = t, respectively and K_{app} and t are the apparent reaction rate constant and time, respectively. From the graphical plot in figure 10, the slope of the linear plots should be equal to the apparent first order rate constant (K_{app}). The K_{app} values give us the degradation rate of Rh.B molecules by the photocatalyst materials under the influence of UV/Vis light. The rate constant K_{app} are listed in table 1. The Rh.B degradation rate constant for $PtSe_2$-GT3 composite were found (6.1×10^{-3}) min^{-1} under visible light, which are much higher than $PtSe_2$-GT1, $PtSe_2$-GT2, and $PtSe_2$-GT4 nanocomposites. These results further confirm that the $PtSe_2$-GT3 nanocomposite is a much more effective catalyst material than the other nanocomposites in our microwave assisted nanocomposites. We further analyze our nanocomposite for the degradation of Texbrite MST-L industrial dye under UV light radiation. After attaining of adsorption desorption equilibrium for 2h. The sample was put under UV light irradiation and six samples were collected periodically during 150 minutes time duration. The

solid was removed by centrifugation and the solution was analyzed by UV-visible spectrometer. From figure 11, we can see that the intensity variation of the Texbrite MST-L with increasing time interval. This further confirms the extraordinary photocatalytic properties of $PtSe_2$-GT3 nanocomposite.

The photocatalytic mechanism was proposed by a number of scientist's worldwide for the utilization of light having wavelength in the range of 400−1000 nm to further explore the photocatalytic mechanisms for graphene based materials. $PtSe_2$ band gap from theoretical and experimental observation were found to be ~1.8eV. This semiconductor material can be excited from its ground state to excited state upon irradiation of visible light. During the catalytic reaction incident light radiation excite electrons from the valance band to conduction band. Thus creating electron hole pair, in the absence of any dopant or support material, most of the electron hole pair recombines and thus lower the catalytic effect. Attachment of $PtSe_2$ on graphene sheet enhances the photocatalytic effect because of the extraordinary absorption and conducting properties of graphene [64-65]. During light irradiation incident photons were absorbed by graphene resulting in emission of photoelectrons and transfer to conduction band of $PtSe_2$. Simultaneously the excited electrons in the conduction band of $PtSe_2$ transfer to graphene sheet and prolong the recombination time. These electrons from the $PtSe_2$ and graphene react with absorbed molecule on the surface of graphene sheet and thus prevent the recombination by improving the catalytic effect [6].

Recently TiO_2 graphene has been found as a visible light photocatalyst material. This wide band gap (3.2 eV) TiO_2 semiconductor material cannot be excited upon visible light irradiation. Modifying TiO_2 nanoparticles with graphene can induce visible-light-responsive photocatalytic activity. The oxygen functionalities on the surface of graphene oxide with unpaired π electrons are bonded with titanium atoms on the surface of TiO_2. These interactions are responsible for the reduction of energy band of graphene-TiO_2 nanocomposites. Therefore, it can be inferred that graphene with unpaired π electrons could be used to modify the TiO_2 surface to manufacture a visible-light-responsive photocatalyst. The enhanced photocatalytic activity of graphene-TiO_2 under visible light illumination is attributed to a red shift of the band edge and a significant reduction of the band gap of the graphene-TiO_2 composite, which consequently allows the enhanced absorption of visible light and efficient transfer of photogenerated electrons

through graphene nanosheets. The addition of graphene induces the light absorption intensity in the visible region. Therefore narrowing of band gap is observed for the composite.

The photocatalytic activity can be further improved by the introduction of heterogeneous system. The transfer of electron between two distinct photocatalyst in the system is the determining process for the decomposition of organic dyes [66]. Under visible light irradiation graphene and $PtSe_2$ are excited and transferred electrons simultaneously. These electrons through graphene sheet interact with VB electrons of TiO_2. The graphene sheet behaves like an electrons sea because of high charge transfer effect. These electrons thus react with VB of catalyst materials and increase the recombination time and will help to improve the catalytic effect. The electrons through graphene sheet will transfer to VB of the TiO_2 in the composite and thus creating a donor level. Thus the attached semiconductor material on graphene sheet acts like a kind of electron absorber in the photocatalytic reaction mechanism [61].

The incident photons have sufficient energy to excite these electrons and transferred to CB of TiO_2. This is because the photogenerated electrons from the $PtSe_2$ photocatalysts accumulate on graphene; the Fermi level of graphene would shift upward and closer to the conduction band of the photocatalyst due to the metallic behavior of graphene. Under the light irradiation the sandwich type structure is advantageous not only to electron injection but also to the hole recovery for both $PtSe_2$ and TiO_2. This unusual photocatalytic activity arises from the positive synergetic effect between the $PtSe_2$ and graphene components in this hybrid cocatalyst, which serve as an electron donor, collector, transporter, and a source of active adsorption sites, respectively [21,13]. The two-dimensional planar conjugation structure in graphene facilitated interfacial charge transfer along the graphene sheet to TiO_2 and subsequently an effective charge separation was achieved. The generated electrons (e^-) react with dissolved oxygen molecules and produce oxygen peroxide radicals $O_2^{\bullet-}$. The positive charge hole (h^+) can react with OH^- derived from H_2O to form hydroxyl radicals $OH^\bullet$. The Rh.B and Texbrite MST-L may be degraded by oxygen peroxide radicals $O_2^{\bullet-}$ and hydroxyl radicals $OH^\bullet$ to CO_2, H_2O and other mineralization products. The proposed mechanism is given in figure 12.

Conclusion:

In this study, we successfully synthesized $PtSe_2$-graphene/TiO_2 nanocomposites by a facile microwave assisted method. TEM images clearly indicate that the TiO_2 nanoparticles are well distributed on surface of transparent graphene sheet supported by $PtSe_2$. The XPS result shows the presence of Pt, Se, C and partial oxygen functional groups on graphene sheet. The XRD results explore that hexagonal $PtSe_2$ and anatase TiO_2 were present. From the DRS results one can observed red shift in overall $PtSe_2$-GT (1-4) samples. These also manifest the visible light response of the nanocomposites. From the UV-visible spectrum it is clear that enhanced catalytic effect was observed for $PtSe_2$-GT3 nanocomposite describing the optimum loading effect of graphene in the composites. It is clearly found that the $PtSe_2$-graphene/TiO_2 nanocomposite can be used as an efficient photocatalyst under UV/Visible light irradiation. It is believed that the positive synergetic effect between the $PtSe_2$ and graphene sheets can efficiently suppress charge recombination, improve interfacial charge transfer, and provide a greater number of active adsorption sites and photocatalytic reaction centers. This high activity is also attributed to the positive synergetic effect of high charge mobility and the observed red shift in the absorption edge of the $PtSe_2$-graphene/TiO_2 nanocomposites.

References:

[1] Y. Zhu, S. Murali, W. Cai, X. Li, J. W. Suk, J. R. Potts, R. S. Ruoff, Graphene and Graphene Oxide: Synthesis, Properties, and Applications, Adv. Mater. 2010, 22, 3906 – 3924.

[2] G. Eda, C. Mattevi, H. Yamaguchi, H. Kim, M. Chhowalla, Insulator to Semimetal Transition in Graphene Oxide, J. Phys. Chem. C 2009, 113, 15768 – 15771.

[3] T. F. Yeh, F. F. Chan, C. T. Hsieh, H. Teng, Graphite Oxide with Different Oxygenated Levels for Hydrogen and Oxygen Production from Water under Illumination: The Band Positions of Graphite Oxide, J. Phys. Chem. C 2011, 115, 22587 – 22597.

[4] Chun Kiang Chua and Martin Pumera, Renewal of sp^2 bonds in graphene oxides *via* dehydrobromination J. Mater. Chem**.**, 2012,**22**, 23227-23231

[5] Y. H. Ng, A. Iwase, A. Kudo, R. Amal, Reducing graphene oxide on a visible-light $BiVO_4$ photocatalyst for an enhanced photoelectrochemical water splitting, J. Phys. Chem. Lett. 2010, 1, 2607 –2612

[6] K. Ullah, L. Zhu, Z. D. Meng, S. Ye, S. Sarkar, W. C. Oh, Synthesis and characterization of novel $PtSe_2$/graphene nanocomposites and its visible light driven catalytic properties, *Journal of Material Science,* (2014) 49:4139–4147

[7] A. Iwase, Y. H. Ng, Y. Ishiguro, A. Kudo, R. Amal, Reduced graphene oxide as a solid-state electron mediator in Z-scheme photocatalytic water splitting under visible Light, J. Am. Chem. Soc. 2011, 133, 11054 –11057

[8] Rajendra C. Pawar, Caroline Sunyong Lee, Single-step sensitization of reduced graphene oxide sheets and CdS nanoparticles on ZnO nanorods as visible-light photocatalysts, Applied Catalysis B: Environmental 144 (2014) 57– 65

[9] K. Ullah, L. Zhu, Z. D. Meng, S. Ye, Q. Sun, W. C. oh, A facile and fast synthesis of novel composite Pt–graphene/TiO_2 with enhanced photocatalytic activity under UV/Visible light, *Chemical Engineering Journal*, 231 76-83 (2013)

[10] Rajendra C. Pawar, Caroline Sunyong Lee, Sensitization of CdS nanoparticles onto reduced graphene oxide (RGO) fabricated by chemical bath deposition method for effective removal of Cr(VI), Materials Chemistry and Physics 141 (2013) 686–693

[11] Nan Zhang, Min-Quan Yang, Zi-Rong Tang, and Yi-Jun Xu, Toward Improving the Graphene–Semiconductor Composite Photoactivity via the Addition of Metal Ions as Generic Interfacial Mediator, ACS Nano, 2014, 8, 623-633.

[12] K. Ullah, S. Ye, L. Zhu, S. B. Jo, W. K. Jang, K. Y. Cho, W. C. Oh, Noble metal doped graphene nanocomposites and its study of photocatalytic hydrogen evolution, *Solid State Sciences*, Volume 31, May 2014, Pages 91-98

[13] Xiang, Q. J. Yu, J. G. Jaroniec, M. Graphene-Based Semiconductor Photocatalysts. Chem. Soc. Rev. 2012, 41, 782−796.

[14] Min-Quan Yang and Yi-Jun Xu, Selective photoredox using graphene-based composite photocatalysts, Physical Chemistry Chemical Physics, 2013, 15, 19102–19118.

[15] Min, S. X. Lu, G. X. Dye-Sensitized reduced graphene oxide photocatalysts for highly efficient visible-light-driven water reduction. J. Phys. Chem. C 2011, 115, 13938−13945.

[16] K. Ullah, S. Ye, L. Zhu, Z. D. Meng, S. Sarkar, W. C. Oh, Microwave assisted synthesis of a noble metal-graphene hybrid photocatalyst for high efficient decomposition of organic dyes under visible light, *Materials Science & Engineering B*, Vol 180 2014, 20-26

[17] An, X. Q. Yu, J. C. Graphene-based photocatalytic composites. RSC Adv. 2011, 1, 1426−1434.

[18] Xiaoyang Pan, Min-Quan Yang, and Yi-Jun Xu, Morphology control, defect engineering and photoactivity tuning of ZnO crystals by graphene oxide – a unique 2D macromolecular surfactant. Physical Chemistry Chemical Physics, 2014, 16, 5589–5599

[19] Han, L. Wang, P. Dong, S. J. Progress in Graphene-based photoactive nanocomposites as a promising class of photocatalyst. Nanoscale 2012, 4, 5814−5825.

[20] Rajendra C. Pawar, Varsha Khare and Caroline Sunyong Lee, Hybrid photocatalysts using graphitic carbon nitride/cadmium sulfide/reduced graphene oxide (g-C3N4/CdS/RGO) for superior photodegradation of organic pollutants under UV and visible light. Dalton Trans., 2014, 43, 12514-12527

[21] Quanjun Xiang and Jiaguo Yu, Graphene-based photocatalysts for hydrogen generation, J. Phys. Chem. Lett. 2013, 4, 753−759

[22] Chen, C. Cai, W. Long, M. Zhou, B. Wu, Y. Wu, D. Feng, Y. Synthesis of visible-light responsive graphene oxide/TiO_2 composites with p/n heterojunction. ACS Nano 2010, 4, 6425−6432.

[23] Yanhui Zhang, Zi-Rong Tang, Xianzhi Fu, and Yi-Jun Xu, Engineering the unique 2D mat of graphene to achieve graphene-TiO_2 nanocomposite for photocatalytic selective transformation: What advantage does graphene have over Its forebear carbon nanotube? ACS Nano, 2010, 4, 7303-7314.

[24] Ze-Da Meng, Shu Ye, Sourav Sarkar, Lei Zhu, Kefayat Ullah and Won-Chun Oh, Review for Graphene based photocatalysis materials, Journal Of Multifunctional Materials & Photoscience 4 (2), December 2013, pp. 103-111

[25] Lee, J. S. You, K. H. Park, C. B. Highly photoactive, low bandgap TiO_2 nanoparticles wrapped by graphene. Adv. Mater. 2012, 24, 1084−1088

[26] Zhang, Y. H. Zhang, N. Tang, Z. R. Xu, Y. J. Graphene transforms wide band gap ZnS to a visible light photocatalyst. The new role of graphene as a macromolecular photosensitizer. ACS Nano 2012, 6, 9777−9789.

[27] Higashi, M. Abe, R. Ishikawa, A. Takata, T. Ohtani, B. Domen, K. Z-scheme overall water splitting on modified-TaON photocatalysts under visible light (l < 500 nm), Chem. Lett., **37**, 138-139 (2008).

[28] Nan Zhang , Yanhui Zhang , Xiaoyang Pan , Min-Quan Yang , and Yi-Jun Xu, Constructing Ternary CdS–Graphene–TiO2 hybrids on the flatland of graphene Oxide with enhanced visible-light photoactivity for selective transformation, Journal of Physical Chemistry C, 2012, 116, 18023-18031

[29] K. Ullah, Z. D. Meng, S. Ye, L. Zhu, W. C. Oh, Synthesis and Characterization of Novel PbS-Graphene/TiO_2 composite with enhanced photocatalytic activity, *Journal of industrial and engineering chemistry*, vol 20 issue 3, 25 may 2014 , 1035-1042.

[30] Nan Zhang, Siqi Liu and Yi-Jun Xu, Recent progress on metal core@semiconductor shell nanocomposites as a promising type of photocatalyst, Nanoscale, 2012, 4, 2227-2238

[31] K. Ullah, S. Ye, S. B. Jo, L. Zhu, K. Y. Cho, W. C. Oh, Optical and photocatalytic properties of novel heterogeneous $PtSe_2$–graphene/TiO_2 nanocomposites synthesized via ultrasonic assisted techniques, Ultrasonics Sonochemistry, 21 (2014) 1849–1857

[32] T. Ghosh, W. C. Oh, Review on reduced graphene oxide by chemical exfoliation method and its simpler alternative of ultrasonication and heat treatment method for obtaining graphene, J. Photocatal. Sci. Volume 3, Issue 1, Pages 17-23, 2012.

[33] Eng-Poh Ng, Darren Tat-Lun Ng, Hussein Awala, Ka-Lun Wong, Svetlana Mintova, Microwave synthesis of colloidal stable AlPO-5 nanocrystals with high water adsorption capacity and unique morphology, Materials Letters Volume 132, 1 October 2014, Pages 126–129

[34] Liangliang Zhang, Xiao Chen, Shaohua Jin, Jingchao Guan, Christopher T. Williams, Zhijian Peng, Changhai Liang**,** Rapid microwaves synthesis of CoSi*x*/CNTs as novel catalytic materials for hydrogenation of phthalic anhydride**,** Journal of Solid State Chemistry**,** Volume 217, September 2014, Pages 105–112

[35] Li Gu, Lei Qian, Ying Lei, Yanyan Wang, Jing Li, Hongyan Yuan, Dan Xiao, Microwave-assisted synthesis of nanosphere-like $NiCo_2O_4$consisting of porous nanosheets and its application in electro-catalytic oxidation of methanol, Journal of Power Sources Volume 261, 1 September 2014, Pages 317–323

[36] K. Ullah, S. Ye, L. Zhu, Z. D. Meng, S. Sarkar, W. C. Oh, Microwave assisted synthesis of a noble metal-graphene hybrid photocatalyst for high efficient decomposition of organic dyes under visible light, Materials Science & Engineering *B*, Vol 180 2014, 20-26

[37] S. D. Perera, R. G. Mariano, K. Vu, N. Nour, O. Seitz, Y. Chabal, and K. J. Balkus, Jr., Hydrothermal synthesis of graphene-TiO_2 nanotube composites with enhanced photocatalytic activity. ACS Catal. 2012, 2, 949−956

[38] Biljana Pejova, Optical phonons in nanostructured thin films composed by zinc blende zinc selenide quantum dots in strong size-quantization regime: Competition between phonon confinement and strain-related effects, Journal of Solid State Chemistry Volume 213, May 2014, Pages 22–31

[39] B.D. Cullity, Elements of X-rays Diffraction, second ed., Addison Wesley Publishing Co, Philippines, 1978, p. 338, Chap. 10

[40] L. Zhua, M. Teo, P.C. Wong, K.C. Wong, I. Narita, F. Ernst, K.A.R. Mitchell, S.A. Campbell, Synthesis, characterization of a $CoSe_2$ catalyst for the oxygen reduction reaction, Applied Catalysis A: General 386 (2010) 157–165

[41] Maytal Caspary Toroker, Dalal K. Kanan, Nima Alidoust, Leah Y. Isseroff, Peilin Liao and Emily A. Carter, First principles scheme to evaluate band edge positions in potential transition metal oxide photocatalysts and photo electrodes, Phys. Chem. Chem. Phys. 13, 16644-16654 (2011)

[42] Houlong L. Zhuang and Richard G. Hennig, Computational search for single-layer transition-Metal Dichalcogenide Photocatalysts, J. Phys. Chem. C, 2013, *117* (40), pp 20440–20445

[43] Quanjun Xiang, Jiaguo Yu, and Mietek Jaroniec, Synergetic effect of MoS_2 and graphene as cocatalysts for enhanced photocatalytic H_2 production activity of TiO_2 nanoparticles, J. Am. Chem. Soc. 2012, 134, 6575−6578

[44] Jeong, H. K. Noh, H. J. Kim, J. Y. Jin, M. H. Park, C. Y. Lee, Y. H., X-ray absorption spectroscopy of graphite oxide. EPL, 82 (2008), pp. 67004–67005

[45] Daniel R. Dreyer, Sungjin Park, Christopher W. Bielawski and Rodney S. Ruoff, The chemistry of graphene oxide, Chem. Soc. Rev., 2010, 39, 228–240

[46] Gao, W. Alemany, L.B. Ci, L. Ajayan, P.M. New insights into the structure and reduction of graphite oxide.Nature Chem. 2009, 1, 403-408

[47] Boukhvalov, D. W. & Katsnelson, M. I. Modeling of graphite oxide. J. Am. Chem. Soc. 130, 10697–10701 (2008)

[48] Zuoli He, Wenxiu Que, Jing Chen, Yucheng He, Gangfeng Wang, Surface chemical analysis on the carbon-doped mesoporous TiO_2 photocatalysts after post-thermal treatment: XPS and FTIR characterization, Journal of Physics and Chemistry of Solids**,** Volume 74, Issue 7, July 2013, Pages 924–928

[49] Ernesto Paparazzo On the interpretation of XPS spectra of metal (Pt, Pt–Sn) nanoparticles/graphene systems, Carbon Volume 63, November 2013, Pages 578–581

[50] E.U. Condon, G.H. Shortley, The theory of atomic spectra, Cambridge University press, Cambridge (1977), pp. 122–124

[51] K.L. Ono, B. Yuan, H. Heinrich, B. Roldan Cuenya, Formation and thermal stability of platinum oxides on size-selected platinum nanoparticles: support effects, J Phys Chem C, 114 (50) (2010), pp. 22119–2213.

[52] Zainab Zafar, Zhen Hua Ni, Xing Wu, Zhi Xiang Shi, Hai Yan Nan, Jing Bai, Li Tao Sun, Evolution of Raman spectra in nitrogen doped graphene, Carbon, 61, (2013) 57 –62

[53] E. Anastassakis, light scattering in transition metal diselenide $CoSe_2$ and $CuSe_2$, Solid State Communications, Vol. 13, pp. 1297—1301, 1973.

[54] Ruey-Chi Wang, Ya-Chun Chen, Shu-Jen Chen, Yu-Ming Chang, Unusual functionalization of reduced graphene oxide for excellent chemical surface-enhanced Raman scattering by coupling with ZnO, Carbon, Volume 70, April 2014, Pages 215–223

[55] S. Ameen, H. K. Seo, M. S. Akhtar, H. S. Shin, Novel graphene/polyaniline nanocomposites and its photocatalytic activity toward the degradation of rose Bengal dye, Chemical Engineering Journal, 210 (2012) 220–228

[56] G. Williams, B. Seger, and P. V. Kamat, Electrocatalytically active graphene-platinum nanocomposites. Role of 2-D Carbon Support in PEM Fuel Cells, J. Phys. Chem. C, 2009, 113 (19), pp 7990–7995

[57] R. Rao, R. Podila, R. Tsuchikawa, J. Katoch, D. Tishler, A. Rao, I M. shigami, Effects of Layer Stacking on the Combination Raman Modes in Graphene, ACS Nano , 2011, 5 (3), 1594–1599.

[58] K. John, D.T. Manolis, D.P. George, N.A. Mariza, S.T. Kostas, G. Sofia, B. Kyriakos, K. Christos, O. Michael, L. Alexis, Highly active catalysts for the photo oxidation of organic compounds by deposition of fullerene onto the MCM-41 surface: A green approach for the synthesis of fine chemicals, Applied Catalysis B: Environmental, 117–118 (2012), pp. 36–48

[59] J. Tauc, R. Grigorovici and A. Vancu, Optical properties and eelectronic sstructure of aamorphous germanium, physica status solidi (b)Volume 15, Issue 2, pages 627–637, 1966

[60] T. Lv, L. Pan, X. Liu, T. Lu, G. Zhu, Z. Sun, C.Q. Sun, One-step synthesis of CdS–TiO_2–chemically reduced graphene oxide composites *via* microwave-assisted reaction for visible-light photocatalytic degradation of methyl orange, Catalysis Science and Technology, 2 (2012) 754–758.

[61] P. Zeng, Q. Zhang, T. Peng, X. Zhang, One-pot synthesis of reduced graphene oxide–cadmium sulfide nanocomposite and its photocatalytic hydrogen production, Physical Chemistry Chemical Physics 13(2011) 21496–21502.

[62] Jingxiang Low, Jiaguo Yu, Qin Li and Bei Cheng, Enhanced visible light photocatalytic activity of plasmonic Ag and graphene Co-modified Bi_2WO_6 nanosheets, Phy.chem.chem.phy, 2014, 16, 1111-1120

[63] K. John, D.T. Manolis, D.P. George, N.A. Mariza, S.T. Kostas, G. Sofia, B. Kyriakos, K. Christos, O. Michael, L. Alexis, Highly active catalysts for the photo oxidation of organic compounds by deposition of fullerene onto the MCM-41 surface: A green approach for the synthesis of fine chemicals, Applied Catalysis B: Environmental, 117–118 (2012), pp. 36–48

[64] Kim, H. Moon, G. Monllor Satoca, D. Park, Y. Choi, W. Solar Photo conversion Using Graphene/TiO_2 Composites: Nano graphene Shell on TiO2 Core versus TiO2 Nanoparticles on Graphene Sheet. J. Phys. Chem. C 2012, 116, 1535−1543.

[65] Zhang, N. Zhang, Y. H. Xu, Y. J. Recent Progress on Graphene-Based Photocatalysts: Current Status and Future Perspectives. Nanoscale 2012, 4, 5792−5813.

[66] Chen, C. Cai, W. Long, M. Zhou, B. Wu, Y. Wu, D. Feng, Y. Synthesis of Visible-Light Responsive Graphene Oxide/TiO_2 Composites with p/n Heterojunction. ACS Nano 2010, 4, 6425−6432.

Figure Caption:

Figure 1. XRD pattern of bare $PtSe_2$ and $PtSe_2$-graphene/TiO_2 composites

Figure 2. EDX spectra $PtSe_2$-graphene/TiO_2 nanocomposites

Figure 3. SEM micrographs of $PtSe_2$-GT3 with different magnifications

Figure 4. TEM Images of $PtSe_2$-GT3 (a) 0.2μm (b) 100 nm (c) 50nm (d-e) 50 nm

Figure 5. XPS results of $PtSe_2$-GT3 nanocomposite (a) C1s (b) Ti2p (c) O1s (d) Se3d (e) Pt4f (f) survey scan spectra

Figure 6. Raman spectra ; (A) GO (B); (a) $PtSe_2$-GT1(b) $PtSe_2$-GT2 (c) $PtSe_2$-GT4 (d) $PtSe_2$-GT3

Figure 7. Diffuse reflectance spectra (DRS) (a) $PtSe_2$-GT1 (b) $PtSe_2$-GT2 (c) $PtSe_2$-GT4 (d) $PtSe_2$-GT3 (e) TiO_2

Figure 8. Transform Kubelka Munk function verses photon energy; (a) $PtSe_2$-GT1 (b) $PtSe_2$-GT2 (c) $PtSe_2$-GT4 (d) $PtSe_2$-GT3: Inset (e) TiO_2

Figure 9. UV/Vis absorption spectra for the Rh.B degradation by $PtSe_2$-graphene/TiO_2 under visible light (a) $PtSe_2$-GT1 (b) $PtSe_2$-GT3 (c) $PtSe_2$-GT4 (d) Plot of Rh.B degradation efficiency v/s irradiation time

Figure 10. Apparent first order kinetics of Rh.B degradation over $PtSe_2$-GT(1- 4) nanocomposites under visible light

Figure 11. UV-vis absorption spectra for the Texbrite MST-L degradation by $PtSe_2$-GT3 under UV light irradiation.

Figure 12. Charge transfer mechanism at the interface of $PtSe_2$ and graphene supportted by TiO_2 catalyst nanocomposites

Scheme 1. Microwave reaction chamber for the synthesis of $PtSe_2$-graphene/TiO_2 nanocomposites

Table.1 Elemental weight %, photocatalytic degradation rate (k_{app}) constant and E_g of $PtSe_2$-graphene/TiO_2 under UV/Visible light

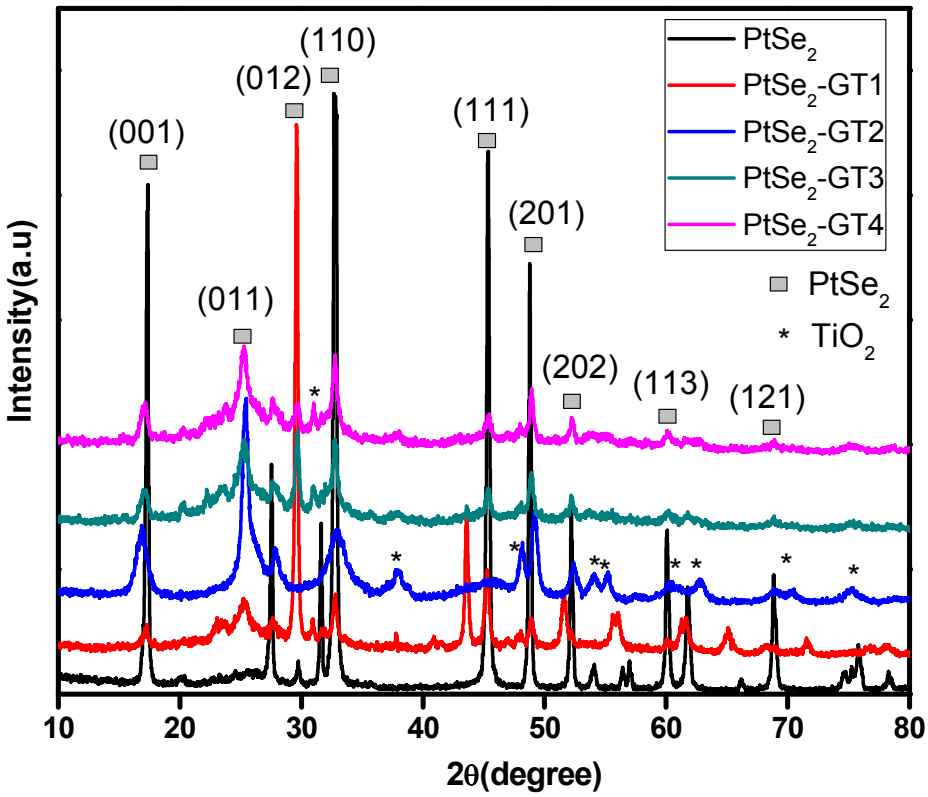

Figure 1. XRD pattern of $PtSe_2$-graphene/TiO_2 composites

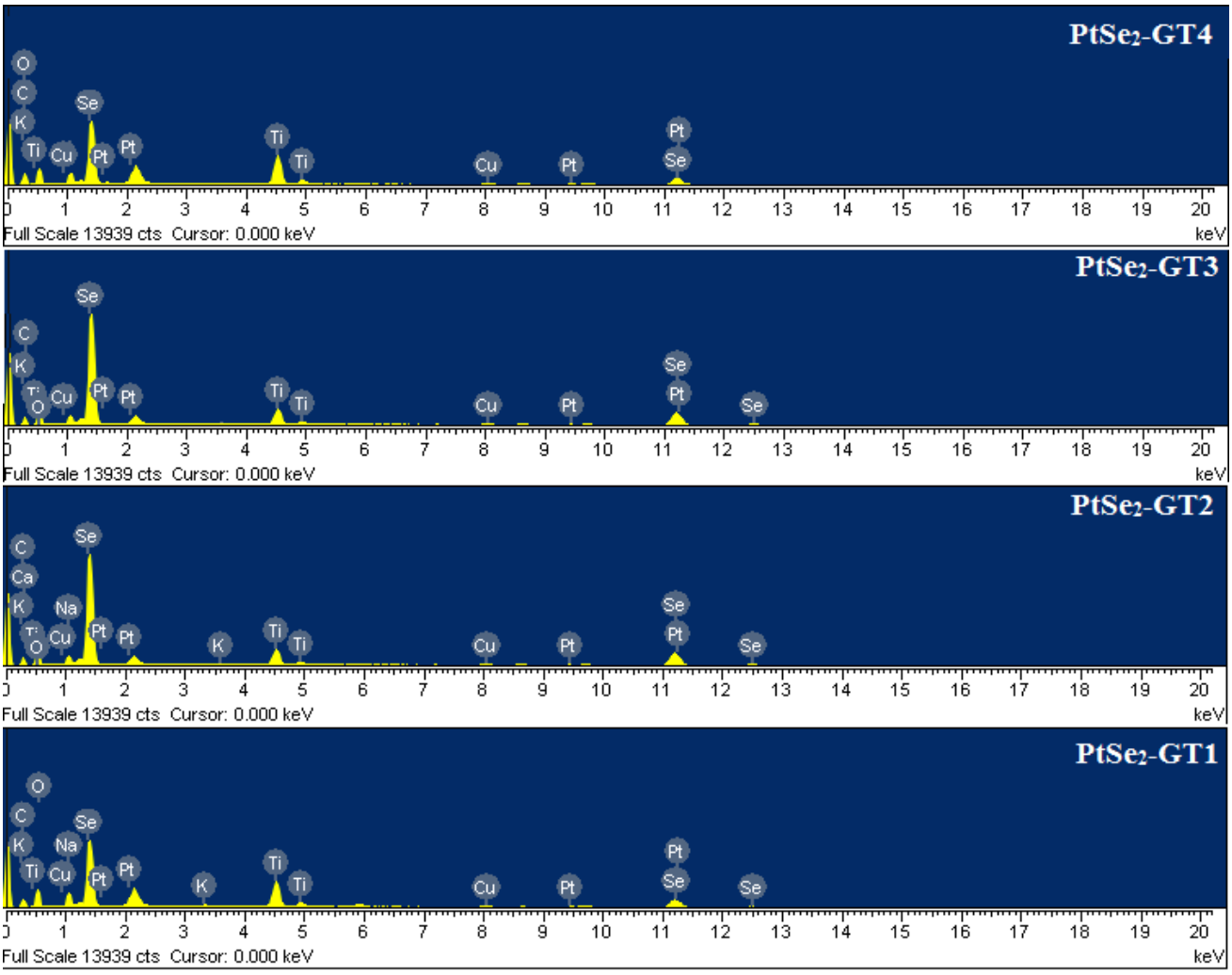

Figure 2. EDX spectra $PtSe_2$-graphene/TiO_2 nanocomposites

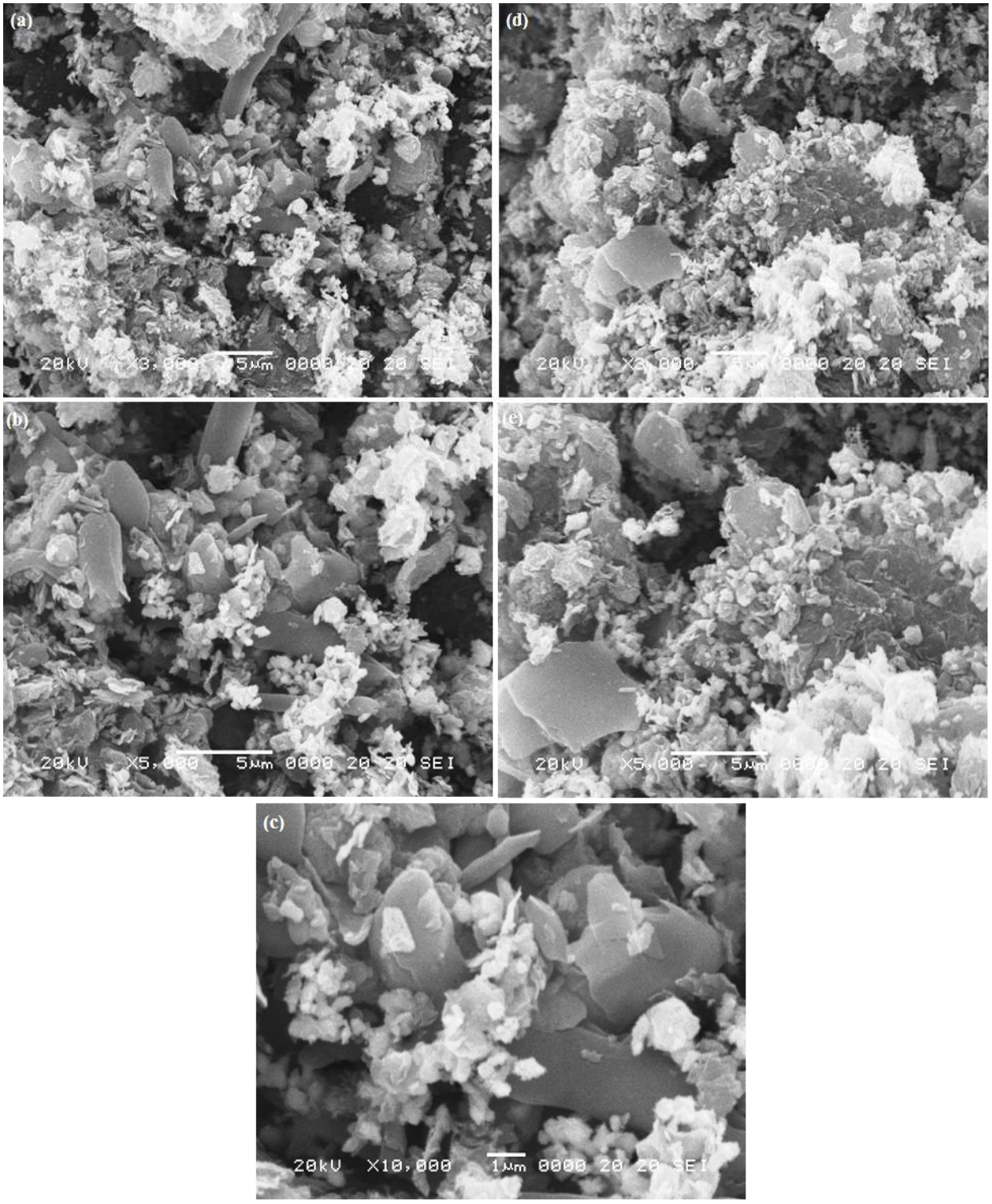

Figure 3. SEM micrographs of $PtSe_2$-GT3 with different magnifications

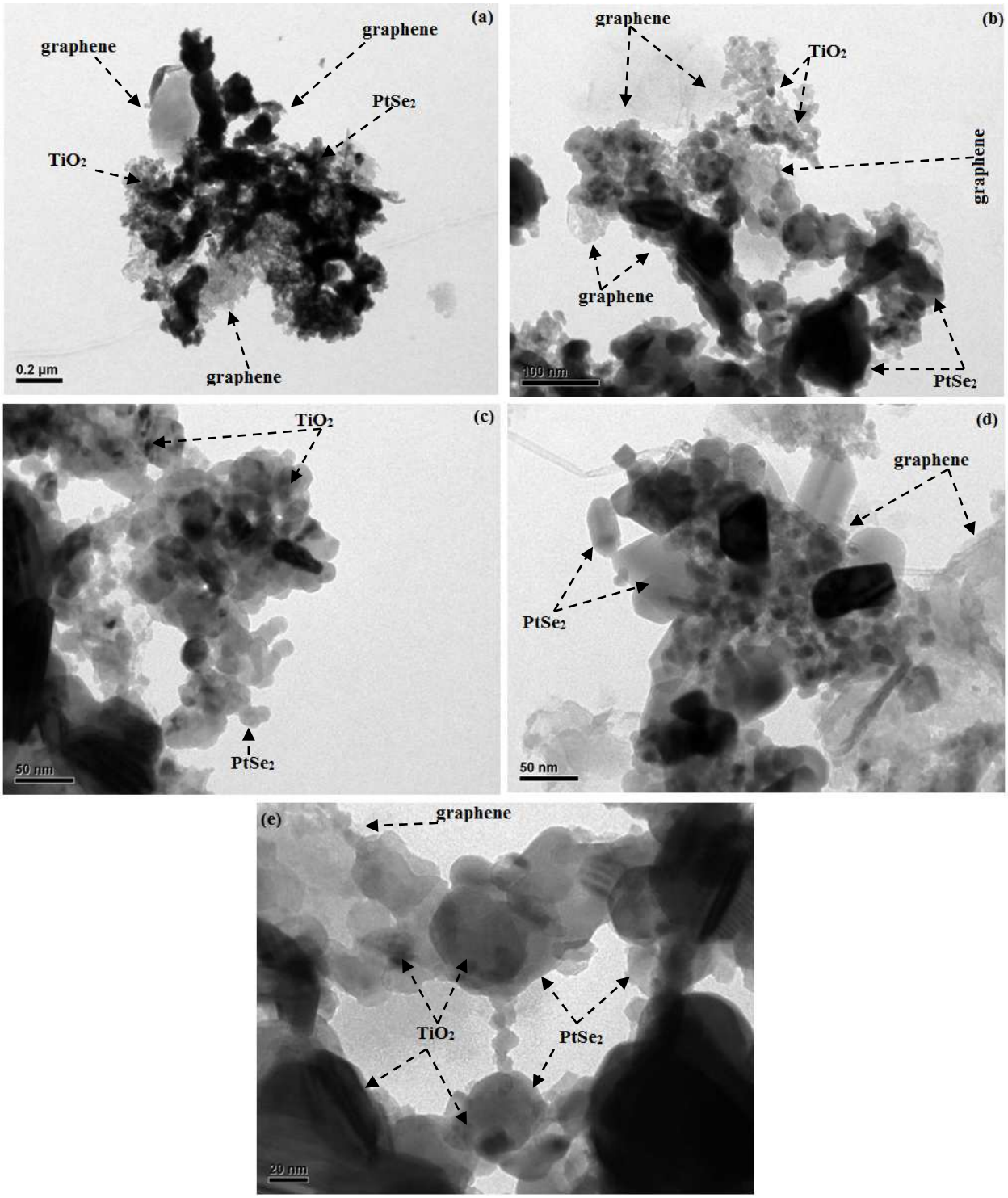

Figure 4. TEM Images of $PtSe_2$-GT3 (a) 0.2µm (b) 100 nm (c-d) 50nm (e) 20 nm

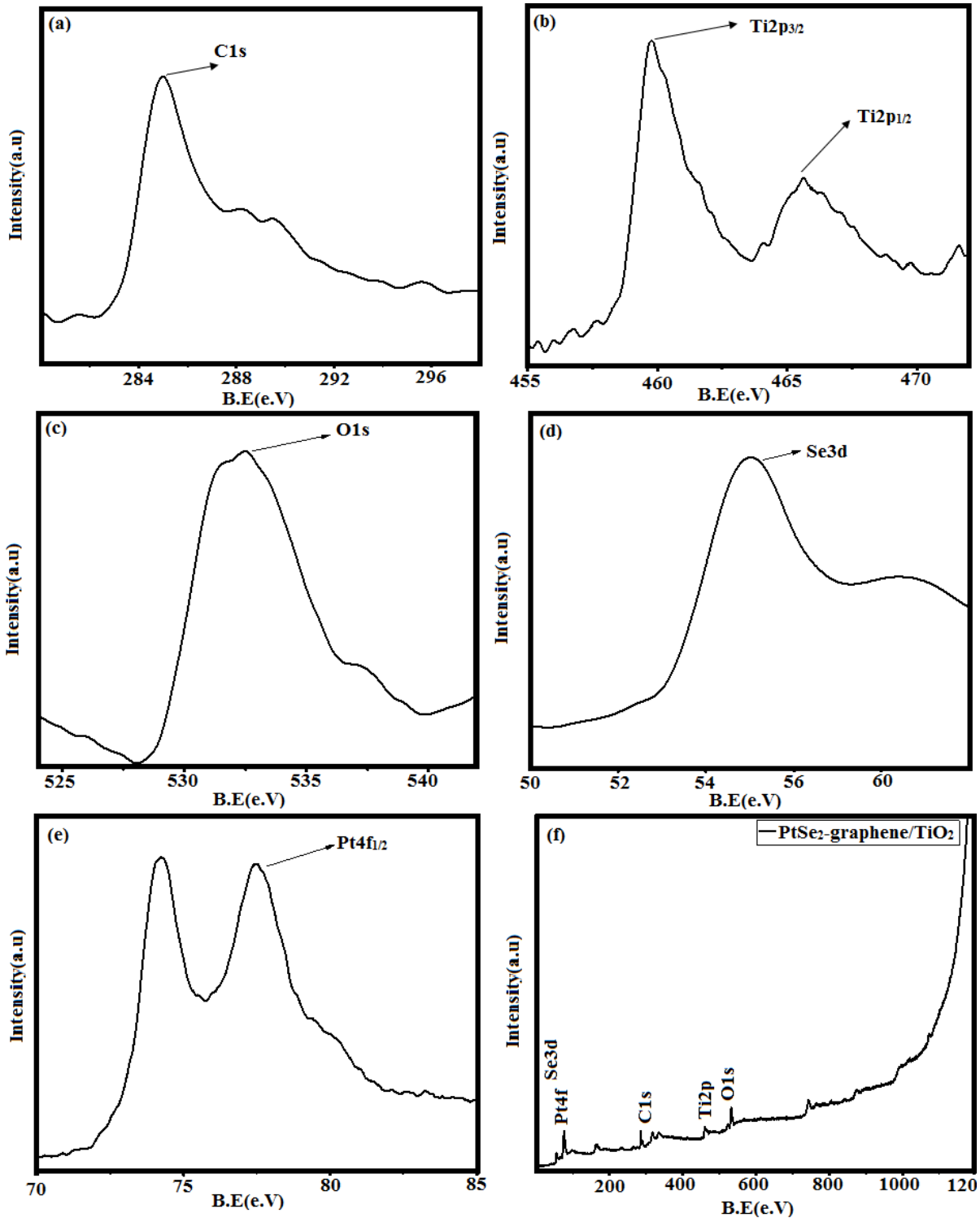

Figure 5. XPS results of $PtSe_2$-GT3 nanocomposite (a) C1s (b) Ti2p (c) O1s (d) Se3d (e) Pt4f (f) survey scan spectra

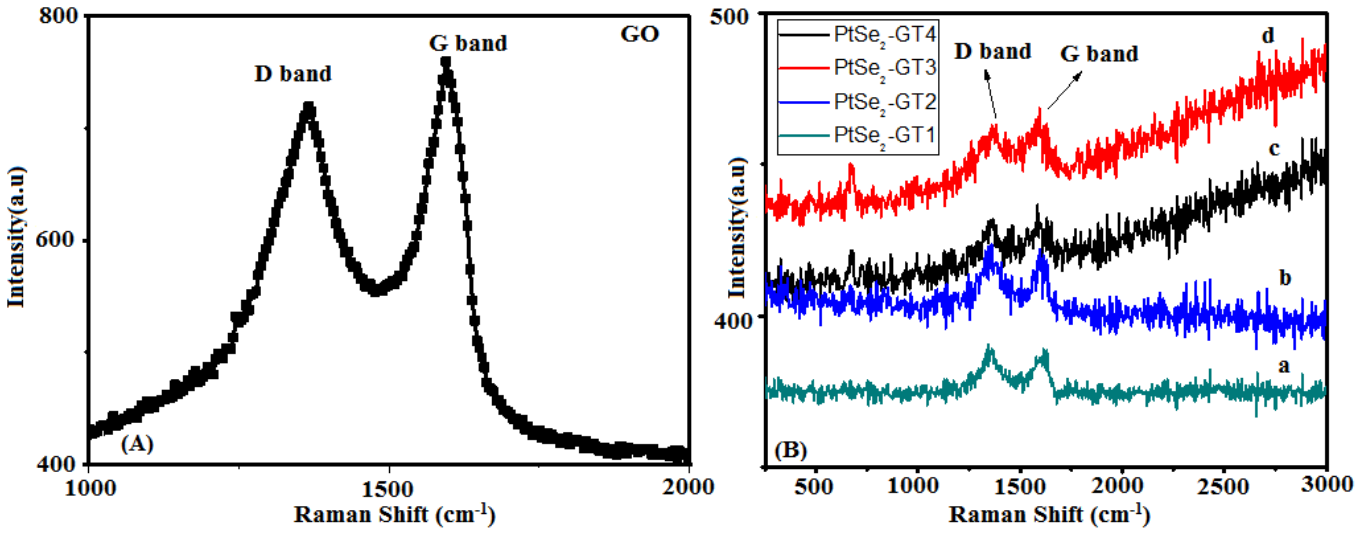

Figure 6. Raman spectra ; (A) GO (B); (a) $PtSe_2$-GT1(b) $PtSe_2$-GT2 (c) $PtSe_2$-GT4 (d) $PtSe_2$-GT3

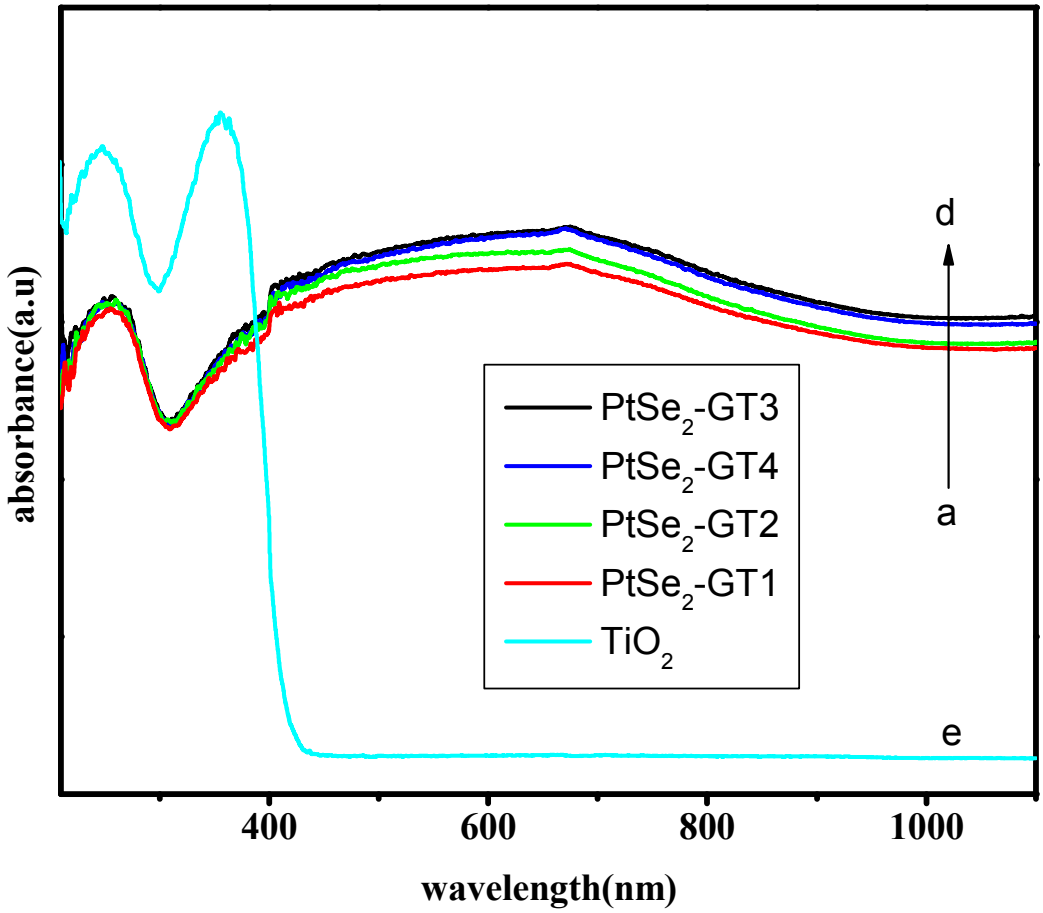

Figure 7. Diffuse reflectance spectra (DRS) (a) $PtSe_2$-GT1 (b) $PtSe_2$-GT2 (c) $PtSe_2$-GT4 (d) $PtSe_2$-GT3 (e) TiO_2

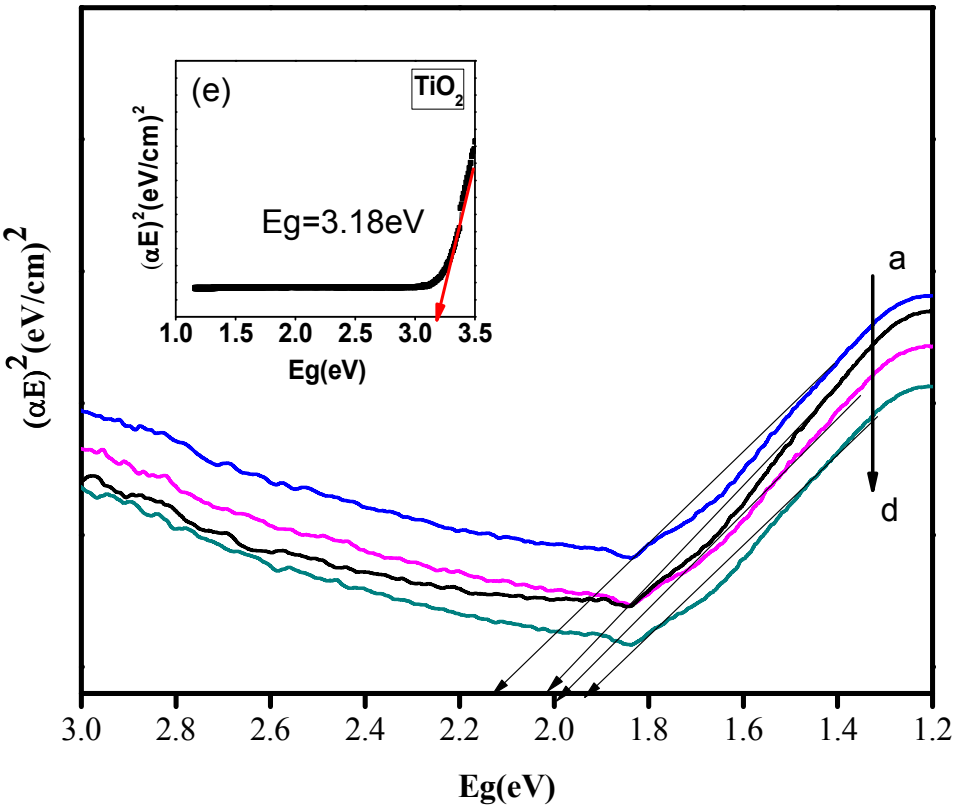

Figure 8. Transform Kubelka Munk function verses photon energy; (a) $PtSe_2$-GT1 (b) $PtSe_2$-GT2 (c) $PtSe_2$-GT4 (d) $PtSe_2$-GT3: Inset (e) TiO_2

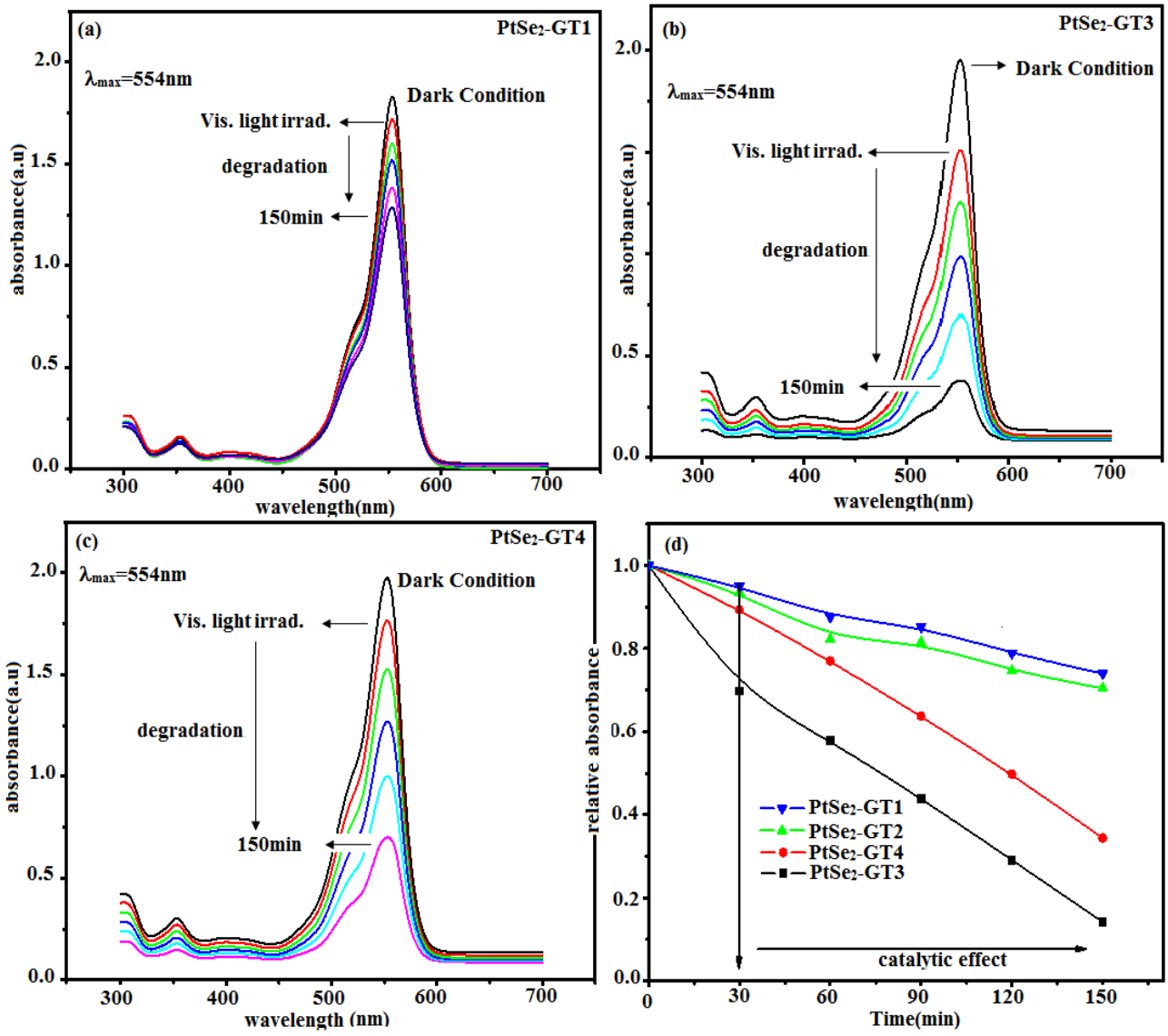

Figure 9. UV/Vis absorption spectra for the Rh.B degradation by $PtSe_2$-graphene/TiO_2 under visible light (a) $PtSe_2$-GT1 (b) $PtSe_2$-GT3 (c) $PtSe_2$-GT4 (d) Plot of Rh.B degradation efficiency v/s irradiation time

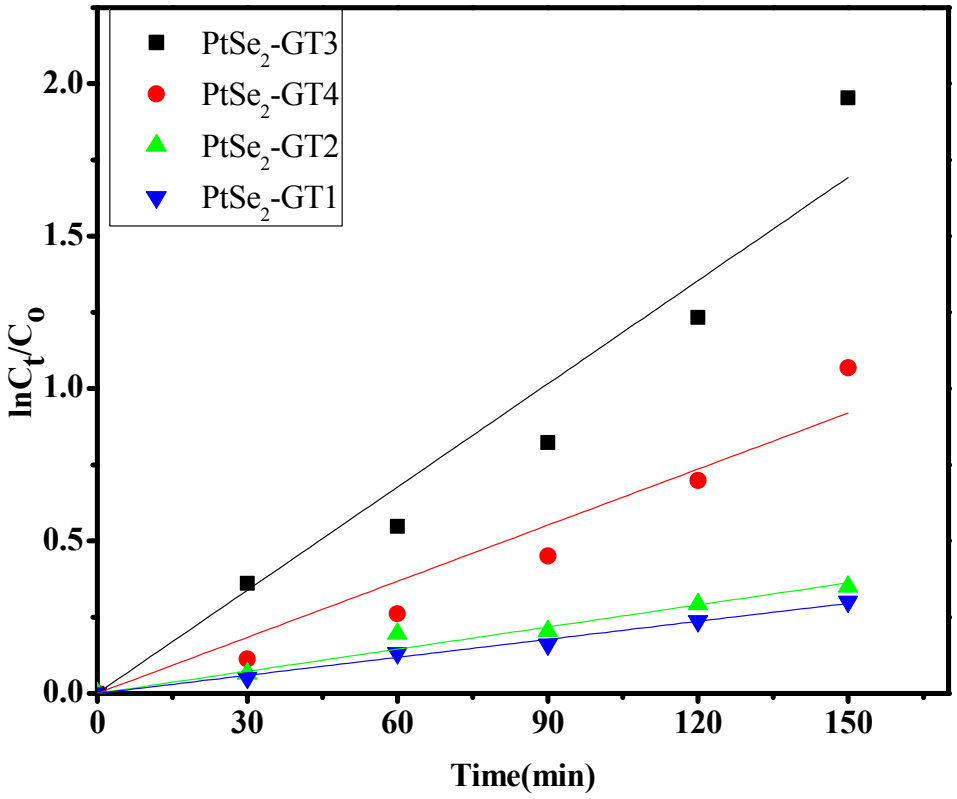

Figure 10. Apparent first order kinetics of Rh.B degradation over $PtSe_2$-GT(1- 4) nanocomposites under visible light

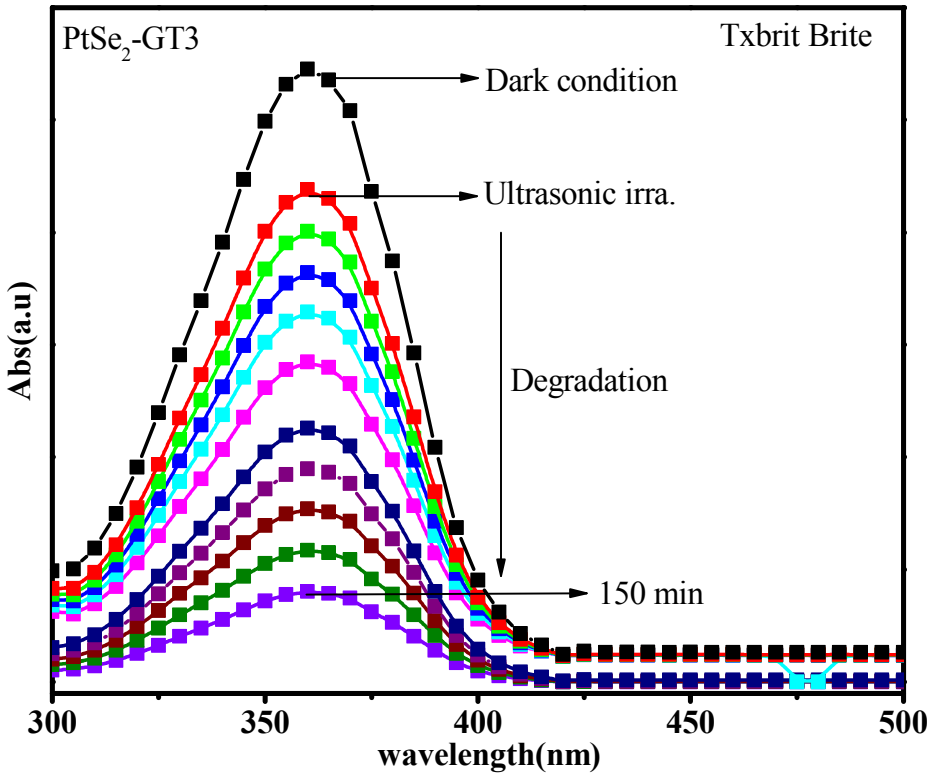

Figure 11. UV-vis absorption spectra for the Texbrite MST-L degradation by $PtSe_2$-GT3 under UV light irradiation.

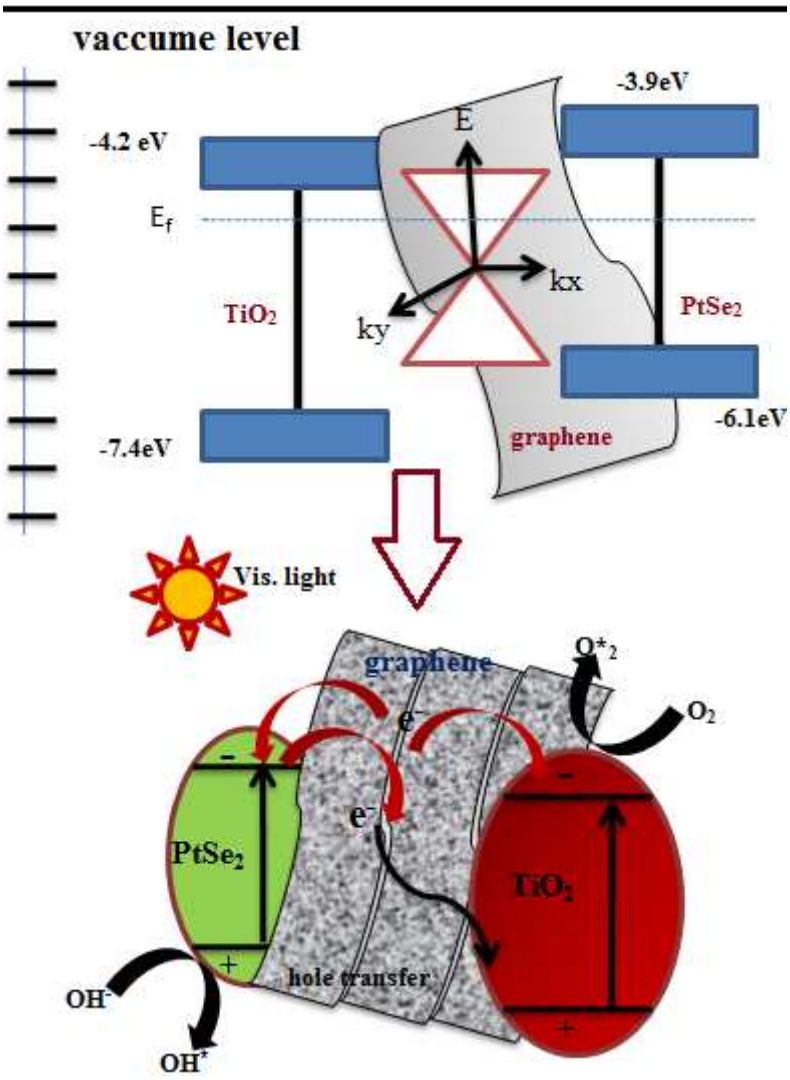

Figure 12. Charge transfer mechanism at the interface of $PtSe_2$ and graphene supportted by TiO_2 catalyst nanocomposites

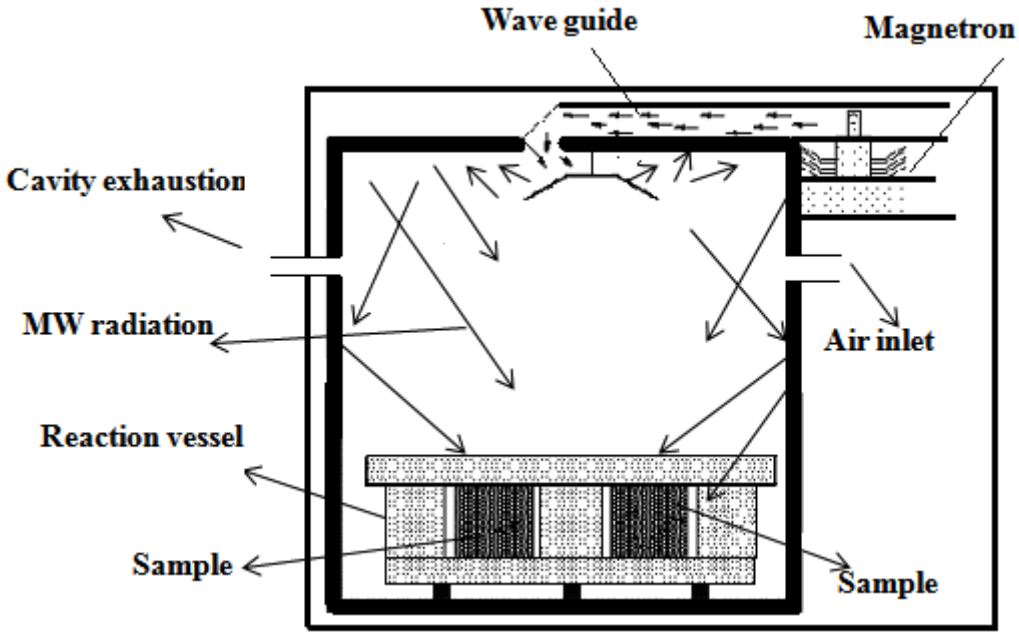

Scheme 1. Microwave reaction chamber for the synthesis of $PtSe_2$-graphene/TiO_2 nanocomposites

Table.1 Elemental weight %, photocatalytic degradation rate (k_{app}) constant and E_g of $PtSe_2$-graphene/TiO_2 under UV/Visible light

Samples	**C %**	**O %**	**Ti %**	**Se%**	**Pt %**	**Other %**	**K_{app}(min^{-1}) Vis light**	**Band Gap(eV)**
$PtSe_2$-GT1	70.2	9.78	10.6	3.6	4.9	0.92	1.70×10^{-3}	2.20
$PtSe_2$-GT2	69.54	9.97	11	4.98	3.34	1.17	1.8×10^{-3}	2.10
$PtSe_2$-GT3	64.13	13.86	10.5	5.51	5.34	0.66	6.1×10^{-3}	1.91
$PtSe_2$-GT4	57.92	12.37	13.50	10.13	4.5	1.58	2.6×10^{-4}	1.98